Freeze-out Dynamics via Charged Kaon Femtoscopy in $\sqrt{s_{NN}}$=200 GeV Central Au+Au Collisions

L. Adamczyk,[1] J. K. Adkins,[23] G. Agakishiev,[21] M. M. Aggarwal,[34] Z. Ahammed,[53] I. Alekseev,[19] J. Alford,[22] C. D. Anson,[31] A. Aparin,[21] D. Arkhipkin,[4] E. Aschenauer,[4] G. S. Averichev,[21] J. Balewski,[26] A. Banerjee,[53] Z. Barnovska,[14] D. R. Beavis,[4] R. Bellwied,[49] M. J. Betancourt,[26] R. R. Betts,[10] A. Bhasin,[20] A. K. Bhati,[34] Bhattarai,[48] H. Bichsel,[55] J. Bielcik,[13] J. Bielcikova,[14] L. C. Bland,[4] I. G. Bordyuzhin,[19] W. Borowski,[45] J. Bouchet,[22] A. V. Brandin,[29] S. G. Brovko,[6] E. Bruna,[57] S. Bültmann,[32] I. Bunzarov,[21] T. P. Burton,[4] J. Butterworth,[40] H. Caines,[57] M. Calderón de la Barca Sánchez,[6] D. Cebra,[6] R. Cendejas,[35] M. C. Cervantes,[47] P. Chaloupka,[13] Z. Chang,[47] S. Chattopadhyay,[53] H. F. Chen,[42] J. H. Chen,[44] J. Y. Chen,[9] L. Chen,[9] J. Cheng,[50] M. Cherney,[12] A. Chikanian,[57] W. Christie,[4] P. Chung,[14] J. Chwastowski,[11] M. J. M. Codrington,[48] R. Corliss,[26] J. G. Cramer,[55] H. J. Crawford,[5] X. Cui,[42] S. Das,[16] A. Davila Leyva,[48] L. C. De Silva,[49] R. R. Debbe,[4] T. G. Dedovich,[21] J. Deng,[43] R. Derradi de Souza,[8] S. Dhamija,[18] B. di Ruzza,[4] L. Didenko,[4] Dilks,[35] F. Ding,[6] A. Dion,[4] P. Djawotho,[47] X. Dong,[25] J. L. Drachenberg,[52] J. E. Draper,[6] C. M. Du,[24] L. E. Dunkelberger,[7] J. C. Dunlop,[4] L. G. Efimov,[21] M. Elnimr,[56] J. Engelage,[5] K. S. Engle,[51] G. Eppley,[40] L. Eun,[25] O. Evdokimov,[10] R. Fatemi,[23] S. Fazio,[4] J. Fedorisin,[21] R. G. Fersch,[23] P. Filip,[21] E. Finch,[57] Y. Fisyak,[4] C. E. Flores,[6] C. A. Gagliardi,[47] D. R. Gangadharan,[31] D. Garand,[37] F. Geurts,[40] A. Gibson,[52] S. Gliske,[2] O. G. Grebenyuk,[25] D. Grosnick,[52] Y. Guo,[42] A. Gupta,[20] S. Gupta,[20] W. Guryn,[4] B. Haag,[6] O. Hajkova,[13] A. Hamed,[47] L-X. Han,[44] R. Haque,[53] J. W. Harris,[57] J. P. Hays-Wehle,[26] S. Heppelmann,[35] A. Hirsch,[37] G. W. Hoffmann,[48] D. J. Hofman,[10] S. Horvat,[57] B. Huang,[4] H. Z. Huang,[7] P. Huck,[9] T. J. Humanic,[31] G. Igo,[7] W. W. Jacobs,[18] C. Jena,[30] E. G. Judd,[5] S. Kabana,[45] K. Kang,[50] K. Kauder,[10] H. W. Ke,[9] D. Keane,[22] A. Kechechyan,[21] A. Kesich,[6] D. P. Kikola,[37] J. Kiryluk,[25] I. Kisel,[25] A. Kisiel,[54] D. D. Koetke,[52] T. Kollegger,[15] J. Konzer,[37] I. Koralt,[32] W. Korsch,[23] L. Kotchenda,[29] P. Kravtsov,[29] K. Krueger,[2] I. Kulakov,[25] L. Kumar,[22] R. A. Kycia,[11] M. A. C. Lamont,[4] J. M. Landgraf,[4] K. D. Landry,[7] S. LaPointe,[56] J. Lauret,[4] A. Lebedev,[4] R. Lednicky,[21] J. H. Lee,[4] W. Leight,[26] M. J. LeVine,[4] C. Li,[42] W. Li,[44] X. Li,[37] X. Li,[46] Y. Li,[50] Z. M. Li,[9] L. M. Lima,[41] M. A. Lisa,[31] F. Liu,[9] T. Ljubicic,[4] W. J. Llope,[40] R. S. Longacre,[4] X. Luo,[9] G. L. Ma,[44] Y. G. Ma,[44] D. M. M. D. Madagodagettige Don,[12] D. P. Mahapatra,[16] R. Majka,[57] S. Margetis,[22] C. Markert,[48] H. Masui,[25] H. S. Matis,[25] D. McDonald,[40] T. S. McShane,[12] S. Mioduszewski,[47] M. K. Mitrovski,[4] Y. Mohammed,[47] B. Mohanty,[30] M. M. Mondal,[47] M. G. Munhoz,[41] M. K. Mustafa,[37] M. Naglis,[25] B. K. Nandi,[17] Md. Nasim,[53] T. K. Nayak,[53] J. M. Nelson,[3] L. V. Nogach,[36] J. Novak,[28] G. Odyniec,[25] A. Ogawa,[4] K. Oh,[38] A. Ohlson,[57] V. Okorokov,[29] E. W. Oldag,[48] R. A. N. Oliveira,[41] D. Olson,[25] M. Pachr,[13] B. S. Page,[18] S. K. Pal,[53] Y. X. Pan,[7] Y. Pandit,[10] Y. Panebratsev,[21] T. Pawlak,[54] B. Pawlik,[33] H. Pei,[9] C. Perkins,[5] W. Peryt,[54] P. Pile,[4] M. Planinic,[58] J. Pluta,[54] D. Plyku,[32] N. Poljak,[58] J. Porter,[25] A. M. Poskanzer,[25] C. B. Powell,[25] C. Pruneau,[56] N. K. Pruthi,[34] M. Przybycien,[1] P. R. Pujahari,[17] J. Putschke,[56] H. Qiu,[25] S. Ramachandran,[23] R. Raniwala,[39] S. Raniwala,[39] R. L. Ray,[48] C. K. Riley,[57] H. G. Ritter,[25] J. B. Roberts,[40] O. V. Rogachevskiy,[21] J. L. Romero,[6] J. F. Ross,[12] A. Roy,[53] L. Ruan,[4] J. Rusnak,[14] N. R. Sahoo,[53] P. K. Sahu,[16] I. Sakrejda,[25] S. Salur,[25] A. Sandacz,[54] J. Sandweiss,[57] E. Sangaline,[6] A. Sarkar,[17] J. Schambach,[48] R. P. Scharenberg,[37] A. M. Schmah,[25] B. Schmidke,[4] N. Schmitz,[27] T. R. Schuster,[15] J. Seger,[12] P. Seyboth,[27] N. Shah,[7] E. Shahaliev,[21] M. Shao,[42] B. Sharma,[34] M. Sharma,[56] W. Q. Shen,[44] S. S. Shi,[9] Q. Y. Shou,[44] E. P. Sichtermann,[25] R. N. Singaraju,[53] M. J. Skoby,[18] D. Smirnov,[4] N. Smirnov,[57] D. Solanki,[39] P. Sorensen,[4] U. G. deSouza,[41] H. M. Spinka,[2] B. Srivastava,[37] T. D. S. Stanislaus,[52] J. R. Stevens,[26] R. Stock,[15] M. Strikhanov,[29] B. Stringfellow,[37] A. A. P. Suaide,[41] M. C. Suarez,[10] M. Sumbera,[14] X. M. Sun,[25] Y. Sun,[42] Z. Sun,[24] B. Surrow,[46] D. N. Svirida,[19] T. J. M. Symons,[25] A. Szanto de Toledo,[41] J. Takahashi,[8] A. H. Tang,[4] Z. Tang,[42] L. H. Tarini,[56] T. Tarnowsky,[28] J. H. Thomas,[25] A. R. Timmins,[49] D. Tlusty,[14] M. Tokarev,[21] S. Trentalange,[7] R. E. Tribble,[47] P. Tribedy,[53] B. A. Trzeciak,[54] O. D. Tsai,[7] J. Turnau,[33] T. Ullrich,[4] D. G. Underwood,[2] G. Van Buren,[4] G. van Nieuwenhuizen,[26] J. A. Vanfossen, Jr.,[22] R. Varma,[17] G. M. S. Vasconcelos,[8] R. Vertesi,[14] F. Videbæk,[4] Y. P. Viyogi,[53] S. Vokal,[21] S. A. Voloshin,[56] A. Vossen,[18] M. Wada,[48] M. Walker,[26] F. Wang,[37] G. Wang,[7] H. Wang,[4] J. S. Wang,[24] Q. Wang,[37] X. L. Wang,[42] Y. Wang,[50] G. Webb,[23] J. C. Webb,[4] G. D. Westfall,[28] H. Wieman,[25] S. W. Wissink,[18] R. Witt,[51] Y. F. Wu,[9] Z. Xiao,[50] W. Xie,[37] K. Xin,[40] H. Xu,[24] N. Xu,[25] Q. H. Xu,[43] W. Xu,[7] Y. Xu,[42] Z. Xu,[4] Yan,[50] C. Yang,[42] Y. Yang,[24] Y. Yang,[9] P. Yepes,[40] L. Yi,[37] K. Yip,[4] I-K. Yoo,[38] Y. Zawisza,[42] H. Zbroszczyk,[54] W. Zha,[42] J. B. Zhang,[9] S. Zhang,[44] X. P. Zhang,[50] Y. Zhang,[42] Z. P. Zhang,[42] F. Zhao,[7] J. Zhao,[44] C. Zhong,[44] X. Zhu,[50] Y. H. Zhu,[44] Y. Zoulkarneeva,[21] and M. Zyzak[25]

(STAR Collaboration)

[1]*AGH University of Science and Technology, Cracow, Poland*
[2]*Argonne National Laboratory, Argonne, Illinois 60439, USA*
[3]*University of Birmingham, Birmingham, United Kingdom*
[4]*Brookhaven National Laboratory, Upton, New York 11973, USA*
[5]*University of California, Berkeley, California 94720, USA*
[6]*University of California, Davis, California 95616, USA*
[7]*University of California, Los Angeles, California 90095, USA*

[8]Universidade Estadual de Campinas, Sao Paulo, Brazil
[9]Central China Normal University (HZNU), Wuhan 430079, China
[10]University of Illinois at Chicago, Chicago, Illinois 60607, USA
[11]Cracow University of Technology, Cracow, Poland
[12]Creighton University, Omaha, Nebraska 68178, USA
[13]Czech Technical University in Prague, FNSPE, Prague, 115 19, Czech Republic
[14]Nuclear Physics Institute AS CR, 250 68 Řež/Prague, Czech Republic
[15]University of Frankfurt, Frankfurt, Germany
[16]Institute of Physics, Bhubaneswar 751005, India
[17]Indian Institute of Technology, Mumbai, India
[18]Indiana University, Bloomington, Indiana 47408, USA
[19]Alikhanov Institute for Theoretical and Experimental Physics, Moscow, Russia
[20]University of Jammu, Jammu 180001, India
[21]Joint Institute for Nuclear Research, Dubna, 141 980, Russia
[22]Kent State University, Kent, Ohio 44242, USA
[23]University of Kentucky, Lexington, Kentucky, 40506-0055, USA
[24]Institute of Modern Physics, Lanzhou, China
[25]Lawrence Berkeley National Laboratory, Berkeley, California 94720, USA
[26]Massachusetts Institute of Technology, Cambridge, MA 02139-4307, USA
[27]Max-Planck-Institut für Physik, Munich, Germany
[28]Michigan State University, East Lansing, Michigan 48824, USA
[29]Moscow Engineering Physics Institute, Moscow Russia
[30]National Institute of Science Education and Research, Bhubaneswar 751005, India
[31]Ohio State University, Columbus, Ohio 43210, USA
[32]Old Dominion University, Norfolk, VA, 23529, USA
[33]Institute of Nuclear Physics PAN, Cracow, Poland
[34]Panjab University, Chandigarh 160014, India
[35]Pennsylvania State University, University Park, Pennsylvania 16802, USA
[36]Institute of High Energy Physics, Protvino, Russia
[37]Purdue University, West Lafayette, Indiana 47907, USA
[38]Pusan National University, Pusan, Republic of Korea
[39]University of Rajasthan, Jaipur 302004, India
[40]Rice University, Houston, Texas 77251, USA
[41]Universidade de Sao Paulo, Sao Paulo, Brazil
[42]University of Science & Technology of China, Hefei 230026, China
[43]Shandong University, Jinan, Shandong 250100, China
[44]Shanghai Institute of Applied Physics, Shanghai 201800, China
[45]SUBATECH, Nantes, France
[46]Temple University, Philadelphia, Pennsylvania, 19122, USA
[47]Texas A&M University, College Station, Texas 77843, USA
[48]University of Texas, Austin, Texas 78712, USA
[49]University of Houston, Houston, TX, 77204, USA
[50]Tsinghua University, Beijing 100084, China
[51]United States Naval Academy, Annapolis, MD 21402, USA
[52]Valparaiso University, Valparaiso, Indiana 46383, USA
[53]Variable Energy Cyclotron Centre, Kolkata 700064, India
[54]Warsaw University of Technology, Warsaw, Poland
[55]University of Washington, Seattle, Washington 98195, USA
[56]Wayne State University, Detroit, Michigan 48201, USA
[57]Yale University, New Haven, Connecticut 06520, USA
[58]University of Zagreb, Zagreb, HR-10002, Croatia
(Dated: September 27, 2013)

We present measurements of three-dimensional correlation functions of like-sign low transverse momentum kaon pairs from $\sqrt{s_{NN}}$=200 GeV Au+Au collisions. A Cartesian surface-spherical harmonic decomposition technique was used to extract the kaon source function. The latter was found to have a three-dimensional Gaussian shape and can be adequately reproduced by Therminator event generator simulations with resonance contributions taken into account. Compared to the pion one, the kaon source function is generally narrower and does not have the long tail along the pair transverse momentum direction. The kaon Gaussian radii display a monotonic decrease with increasing transverse mass m_T over the interval of $0.55 \leq m_T \leq 1.15$ GeV/c^2. While the kaon radii are adequately described by the m_T-scaling in the outward and sideward directions, in the longitudinal direction the lowest m_T value exceeds the expectations from a pure hydrodynamical model prediction.

I. INTRODUCTION

Analysis of the data collected at the Relativistic Heavy Ion Collider (RHIC) has resulted in the discovery of strongly interacting, almost perfect fluid created in high energy nucleus-nucleus collisions [1–4]. Lattice calculations predict that the transition between normal nuclear matter and this new phase is a smooth crossover [5]. This is consistent with the absence of long source lifetimes which would indicate a first-order phase transition [6]. Moreover, analysis of three-dimensional (3D) two-pion correlation functions, exploiting the novel technique of Cartesian surface-spherical harmonic decomposition of Danielewicz and Pratt [7, 8], revealed significant non-Gaussian features in the pion source function [9]. Furthermore, the extraction of the shape of the pion source function in conjunction with model comparisons has permitted the decoupling of the spatio-temporal observable into its spatial and temporal aspects, and the latter into source lifetime and emission duration. However, an interpretation of pion correlations in terms of pure hydrodynamic evolution is complicated by the significant contributions of resonance decays. A purer probe of the fireball decay could be obtained with kaons which suffer less contribution from long lifetime resonances and have a smaller rescattering cross-section than pions. The lower yields, however, make it difficult to carry out a detailed 3D source shape analysis of kaons. A 1D kaon source image measurement was recently reported by the PHENIX Collaboration [10]. This measurement, however, corresponds to a fairly broad range of the pair transverse momentum $2k_T$ which makes the interpretation more ambiguous. In particular, information about the transverse expansion of the system, contained in the k_T dependence of the emission radii, is lost. The 1D nature of the measurement has also less constraining power on model predictions than would be available from a 3D measurement.

This paper presents a full 3D analysis of the correlation function of midrapidity, low transverse momentum like–sign kaon pairs. The technique used in this paper is similar to that employed in the first 3D extraction of the pion source function [9]. It involves the decomposition of the 3D kaon correlation function into a basis of Cartesian surface-spherical harmonics to yield coefficients, also called moments, of the decomposition which are then fitted with a trial functional form for the 3D source function. The latter is then compared to models to infer the dynamics behind the fireball expansion.

II. EXPERIMENT AND DATASETS

The presented data from Au+Au collisions at $\sqrt{s_{NN}} = 200$ GeV were taken by the STAR Collaboration during the year-2004 and 2007 runs. A total of 4.6 million 0-20% central events were used from year 2004, and 16 million 0-20% central events from year 2007. We also analyzed 6.6 million 0–30% central events from the year 2004 run to compare to

the previously published PHENIX kaon measurements [10]. Charged tracks are detected in the STAR Time Projection Chamber (TPC) [11], surrounded by a solenoidal magnet providing a nearly uniform magnetic field of 0.5 T along the beam direction. The TPC is used both for the tracking of charged particles at midrapidity and particle identification by means of ionization energy loss. The z position of the event vertex is constrained to be $|z| < 30$ cm.

III. SOURCE SHAPE ANALYSIS

A. Correlation moments

The 3D correlation function $C(\mathbf{q}) = N_{\text{same}}(\mathbf{q})/N_{\text{mixed}}(\mathbf{q})$ is constructed as the ratio of the 3D relative momentum distribution, $N_{\text{same}}(\mathbf{q})$, for K^+K^+ and K^-K^- pairs in the same event to that from mixed events, $N_{\text{mixed}}(\mathbf{q})$. Here, $\mathbf{q} = (\mathbf{p_1} - \mathbf{p_2})/2$, where $\mathbf{p_1}$ and $\mathbf{p_2}$ are the momentum 3-vectors of the particles in the pair center-of-mass system (PCMS). The non-commutativity of the Lorentz transformations along non–collinear directions demands that the Lorentz transformation from the laboratory frame to the PCMS is made by first transforming to the pair longitudinally co-moving system (LCMS) along the beam direction and then to the PCMS along the pair transverse momentum. $C(\mathbf{q})$ is flat and normalized to unity over $60 < |\mathbf{q}| < 100\,\text{MeV}/c$.

To obtain the moments, the 3D correlation function $C(\mathbf{q})$, is expanded in a Cartesian harmonic basis [7, 8]

$$C(\mathbf{q}) - 1 \equiv R(\mathbf{q}) = \sum_{l,\alpha_1...\alpha_l} R^l_{\alpha_1...\alpha_l}(q) A^l_{\alpha_1...\alpha_l}(\Omega_{\mathbf{q}}) , \quad (1)$$

where $l = 0, 1, 2, ..., \alpha_i = x, y$ or z, and $A^l_{\alpha_1...\alpha_l}(\Omega_{\mathbf{q}})$ are Cartesian harmonic basis elements ($\Omega_{\mathbf{q}}$ is the solid angle in $\mathbf{q}$ space). $R^l_{\alpha_1...\alpha_l}(q)$, where q is the modulus of $\mathbf{q}$, are Cartesian correlation moments,

$$R^l_{\alpha_1...\alpha_l}(q) = \frac{(2l+1)!!}{l!} \int \frac{d\Omega_{\mathbf{q}}}{4\pi} A^l_{\alpha_1...\alpha_l}(\Omega_{\mathbf{q}}) R(\mathbf{q}). \quad (2)$$

The coordinate axes x-y-z form a right-handed *out-side-long* Cartesian coordinate system. They are oriented so that the z-axis is parallel to the beam direction and x points in the direction of the pair total transverse momentum.

Correlation moments can be calculated from the measured 3D correlation function using Eq. (2). Even moments with $l > 4$ were found to be consistent with zero within statistical uncertainty. As expected from symmetry considerations, the same was also found for odd moments. Therefore in this analysis, the sum in Eq. (1) is truncated at $l = 4$ and expressed in terms of independent moments only. Up to order 4, there are 6 independent moments: $R^0, R^2_{xx}, R^2_{yy}, R^4_{xxxx}, R^4_{yyyy}$ and R^4_{xxyy}. Dependent moments are obtained from independent ones [7, 8].

These independent moments were extracted as a function of q, by fitting the truncated series to the measured 3D correlation function with the moments as free parameters of the
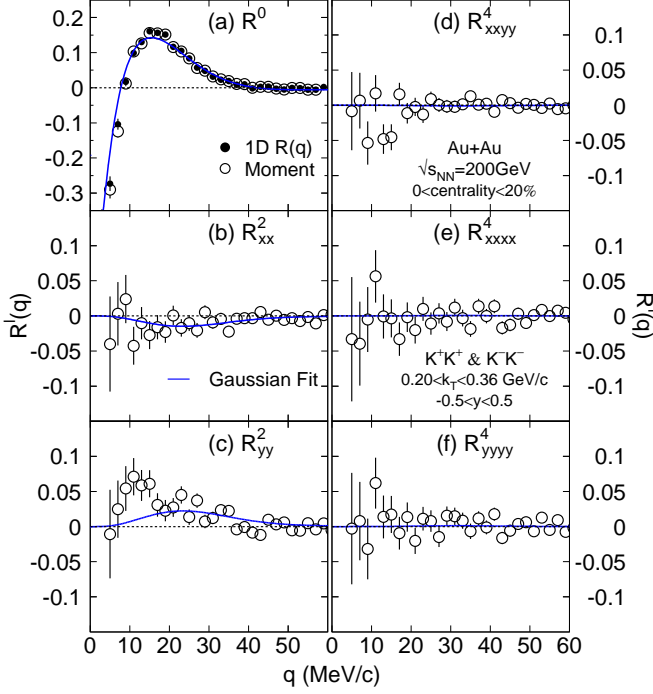
FIG. 1. *(Color online)* Independent correlation moments $R^l(q)$ for orders $l = 0, 2, 4$ for midrapidity, low transverse momentum kaon pairs from the 20% most central Au+Au collisions at $\sqrt{s_{NN}}$=200 GeV. Panel (a) also shows a comparison between $R^0(q)$ and $R(q)$. The error bars are statistical. The solid curves represent results of the Gaussian fit.

fit. The statistical errors on the moments reflect the statistical error on the 3D correlation function. In order to estimate the effect of systematic errors, the 3D correlation function and associated moments were obtained under varying conditions including nominal vs. reverse magnetic field, year 2004 vs. year 2007 data, positively vs. negatively charged kaon pairs and varying kaon sample purities. Although the variations did not introduce any observable systematic deviation in the correlation moments, they have some effect on the parameters of the 3D Gaussian fit of Eq. (4).

Figure 1 shows the independent correlation moments $R^l_{\alpha_1...\alpha_l}$ up to order l=4 (open circles) for midrapidity ($|y|$<0.5), low k_T (0.2<k_T<0.36 GeV/c) kaon pairs produced in the 20% most central Au+Au collisions at $\sqrt{s_{NN}}$=200 GeV; k_T is half the transverse momentum of the pair. In panel (a), $R^0(q)$ is shown along with the 1D correlation function $R(q) = C(q) - 1$ (solid circles); both represent angle-averaged correlation functions, but $R^0(q)$ is obtained from the 3D correlation function via Eq. (2) while $R(q)$ is evaluated directly from the 1D correlation function. The data points have been corrected for the effect of track momentum resolution. The agreement between $R^0(q)$ and $R(q)$ attests to the reliability of the moment extraction technique. Figures 1(b)–(f) show that while second moments are already relatively small compared to their errors, fourth moments are insignificant without any visible trend. This further justifies truncating Eq. (1) at $l = 4$.

B. The 3D source function

The probability of emitting a pair of particles with a pair separation vector $\mathbf{r}$ in the PCMS is given by the 3D source function $S(\mathbf{r})$. It is related to the 3D correlation function $C(\mathbf{q})$ via a convolution integral [6, 12] as

$$C(\mathbf{q}) - 1 \equiv R(\mathbf{q}) = \int \left(|\phi(\mathbf{q}, \mathbf{r})|^2 - 1 \right) S(\mathbf{r}) d\mathbf{r}, \qquad (3)$$

where the relative wave function $\phi(\mathbf{q}, \mathbf{r})$ serves as a six-dimensional kernel, which in our case incorporates Coulomb interactions and Bose-Einstein symmetrization only [8]. Strong final state interactions are assumed to be negligible owing to the small s-wave scattering length ($\sim$0.1 fm) of two identical kaons [13]. Hence, no correction to the measured correlation function for Coulomb and other final-state interaction effects is required. Analogously to Eq. (1), the source function can be expanded in Cartesian harmonics basis elements as $S(\mathbf{r}) = \sum_{l,\alpha_1...\alpha_l} S^l_{\alpha_1...\alpha_l}(r) A^l_{\alpha_1...\alpha_l}(\Omega_{\mathbf{r}})$. Equation (3) can then be rewritten in terms of the independent moments [7, 8].

The 3D source function can be extracted by directly fitting the 3D correlation function with a trial functional form for $S(\mathbf{r})$. Because the 3D correlation function has been decomposed into its independent moments, this corresponds to a simultaneous fit of the six independent moments with the trial functional form. A four-parameter fit to the independent moments with a 3D Gaussian trial function,

$$S^G(r_x, r_y, r_z) = \frac{\lambda}{(2\sqrt{\pi})^3 R_x R_y R_z} \exp[-(\frac{r_x^2}{4R_x^2} + \frac{r_y^2}{4R_y^2} + \frac{r_z^2}{4R_z^2})],$$
$$(4)$$

yields a $\chi^2/ndf = 1.7$. The correlation strength parameter λ represents the integral short-distance contribution to the source function [14]. Figure 1 shows the fit as solid curves, making it evident that the quality of the fit is predominantly driven by the relatively small errors of $R^0(q)$. The values of the Gaussian radii and the amplitude (R_x, R_y, R_z, λ) are listed in Table I.

Figure 2(a)–(c) illustrate the kaon correlation function profiles (circles) in the x, y and z directions ($C(q_x) \equiv C(q_x, 0, 0)$, $C(q_y) \equiv C(0, q_y, 0)$ and $C(q_z) \equiv C(0, 0, q_z)$), respectively, obtained by summation of the relevant correlation terms $C^l_{\alpha_1...\alpha_l}(\mathbf{q}) = \delta_{l,0} + R^l_{\alpha_1...\alpha_l}(q) A^l_{\alpha_1...\alpha_l}(\Omega_{\mathbf{q}})$ up to order l=4. The peak at $q\approx$20 MeV/c is coming from an expected interplay of Coulomb repulsion at $q\rightarrow$0 and Bose-Einstein enhancement. The correlation profiles from the data are well represented by the corresponding correlation profiles from the Gaussian fit (line). Hence, the trial Gaussian shape for the kaon source function seems to capture the essential components of the actual source function.

Figure 3(a)–(c) depict the extracted source function profiles in the x, y and z directions ($S(r_x) \equiv S(r_x, 0, 0)$, $S(r_y) \equiv S(0, r_y, 0)$ and $S(r_z) \equiv S(0, 0, r_z)$) obtained via the 3D Gaussian fit (dots) to the correlation moments. The two solid curves around the Gaussian source function profiles represent the error band arising from the statistical and systematic errors
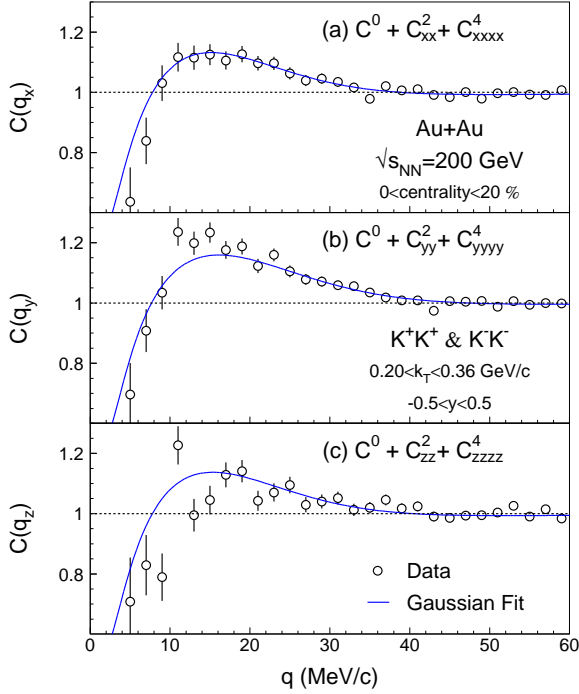
FIG. 2. *(Color online)* Kaon correlation function profiles (circles) for midrapidity, low transverse momentum kaon pairs from the 20% most central Au+Au collisions at $\sqrt{s_{NN}}$=200 GeV (a) $C(q_x) \equiv C(q_x,0,0)$, (b) $C(q_y) \equiv C(0,q_y,0)$ and (c) $C(q_z) \equiv C(0,0,q_z)$ in the x, y and z directions. The curves denote the Gaussian fit profiles.
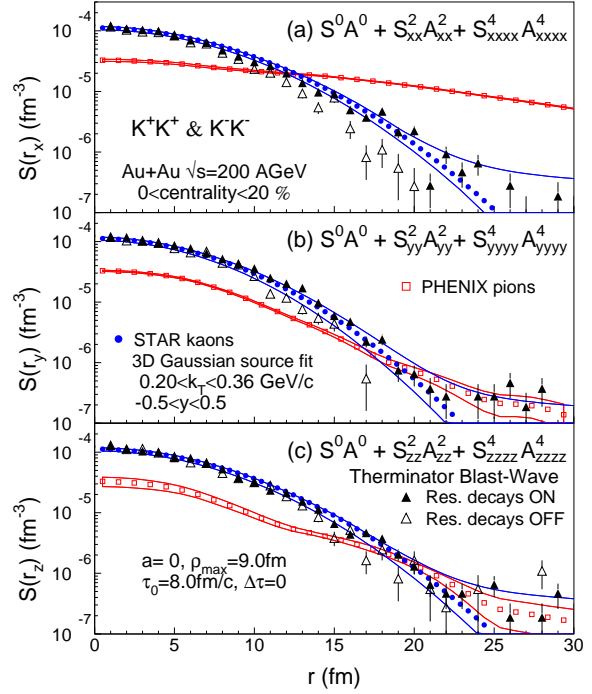

FIG. 3. *(Color online)* Kaon source function profiles extracted from the data (solid circles with error band) and 3D pion source function (squares) from PHENIX [9] together with Therminator model calculation for kaons with indicated parameter values (triangles).

on the 3D Gaussian fit parameters, as well as the uncertainty from the source shape assumption estimated using a double-Gaussian fit. Note that the latter becomes important for large r values only.

C. Expansion dynamics and model comparison

The source function profile $S(r_y)$ in the *side* direction reflects the mean transverse geometric size of the emission source, while the source lifetime determines the extent of the source function profile $S(r_z)$ in the *long* direction. Being in the direction of the total pair transverse momentum (hence the direction of Lorentz boost from the LCMS to PCMS frame), the source function profile in the *out* direction $S(r_x)$ is characterized by the kinematic Lorentz boost, mean transverse geometric size as well as source lifetime and particle emission duration. To disentangle these various contributions, the Monte Carlo event generator Therminator [15] is used to simulate the source breakup and emission dynamics.

The basic ingredients of the Therminator model employed in the analysis are (1) Bjorken assumption of longitudinal boost invariance; (2) blast-wave (BW) expansion in the transverse direction with transverse velocity profile semilinear in transverse radius ρ [16], $v_r(\rho) = (\rho/\rho_{max})/(\rho/\rho_{max} + v_t)$, where v_t=0.445 is obtained from BW fits to particle spectra [17]; (3) after a proper lifetime τ, a thermal emission of

particles takes place from the source elements distributed in a cylinder of infinite longitudinal size and finite transverse dimension ρ_{max}. At the point of source breakup, all particle emission is collectively viewed as happening from a freeze-out hypersurface defined in the ρ-τ plane as $\tau = \tau_0 + a\rho$. Hence, particles which are emitted from a generic source element with coordinates (z,ρ) will have emission time t in the laboratory frame given by $t^2 = (\tau_0 + a\rho)^2 + z^2$.

Note that the BW mode of fireball expansion means that $a = 0$ [18] making τ independent of ρ. Each source element is thus defined by only one value of the proper breakup time $\tau = \tau_0$ and all particle emission from this source element happens instantaneously in the rest frame of the source element and the proper emission duration $\Delta\tau$ is set to 0. Later, we also discuss another choice for parameter a which was used to describe the pion data [9].

Using a set of thermodynamic parameters previously tuned to fit charged pion and kaon spectra [18], midrapidity kaon pairs at low k_T were obtained from Therminator with all known resonance decay processes on and off. They were then boosted to the PCMS to obtain source function profiles for comparison with corresponding profiles from the data.

Figures 3(a)–(c) indicate that the 3D source function generated by the Therminator model in the BW mode (solid triangles) with τ_0=8.0±0.5 fm/c, ρ_{max}=9.0±0.5 fm and other previously tuned parameters [17, 18], reproduces the experimentally extracted source function profiles $S(r_x)$, $S(r_y)$ and $S(r_z)$. The calculations also show that the source function exclud-

ing the contribution of resonances (open triangles) is narrower than the experimentally observed Gaussian. However, they do not allow us to draw a firm conclusion concerning the value of parameter a. Besides the Therminator default $a=0$, we tested the value $a=-0.5$, the same as used in Ref. [9] to describe the pion data. Our simulations with $a=-0.5$ and the other parameters fixed, underestimate the source function $S(r_z)$ already for $r>5$ fm but do not show any change in $S(r_x)$ and $S(r_y)$. Substantial improvement can be achieved if we allow at the same time τ_0 to increase from 8 to ~10.5 fm/c. The latter value is, however, considerably bigger than $\tau_0=8.5$ fm/c reported in [9] for the pions. Given these uncertainties, the scenario when kaon freeze-out occurs in the source element rest frame from a hypersurface devoid of any space-time correlation ($a=0$) is only marginally favored over the one where the emission occurs from the outer surface of the fireball inwards ($a<0$).

Although most of the extracted parameters of the expanding fireball are consistent with those obtained from two-pion interferometry [9], the 3D source function shapes for kaons and pions are very different. This is illustrated in Figs 3 (a)–(c) which compares the correlation profiles for midrapidity kaons (circles) with those for midrapidity pions (squares) reported by the PHENIX Collaboration [9] for the same event centrality and transverse momentum selection. The kaon source function profiles are generally narrower in width than those for pions. Moreover, in contrast to the case for pions, a long tail is not observed in the kaon $S(r_x)$ (i.e. along the pair's total transverse momentum). Compared to the pion case where a prominent cloud of resonance decay pions determines the source-function tail profiles in *out* and *long* directions [9], the narrower shape observed for the kaons indicates a much smaller role of long-lived resonance decays and/or of the exponential emission duration width $\Delta\tau$ on kaon emission.

IV. k_T–DEPENDENCE

Further insight into expanding fireball dynamics can be obtained by studying the k_T–dependence of the kaon Gaussian radii in LCMS. To achieve this goal, in addition to the lowest momentum bin ($0.2<k_\mathrm{T}<0.36$ GeV/c), we have also analyzed the kaon pairs with $0.36<k_\mathrm{T}<0.48$ GeV/c. The analysis was carried out for the 30% most central Au+Au collisions at $\sqrt{s_{NN}}$=200 GeV. This wider centrality cut enabled us to compare our results to the PHENIX kaon data points obtained at higher k_T but at the same centrality [10]. A 4–parameter fit to the two sets of independent moments with a Gaussian function Eq. (4) yields a χ^2/ndf of 1.1 and 1.3 respectively. The three Gaussian radii and the amplitude obtained from this fit are listed in Table I. Note that the overall normalization of $S^G(r_x, r_y, r_z)$ may also be affected by systematic factors not included in this fit. While the value of λ for the 0–20% centrality data is only marginally smaller than that of Ref. [10], the analysis of the 30% most central collisions restricted to year 2004 data uses looser purity cuts, thus yielding substantially smaller λ. Additional dilution of the correlation strength is expected from the $\phi \to K^+K^-$ decays, which is, however, limited by the ϕ decay length of ~11 fm in PCMS [19]. Cal-
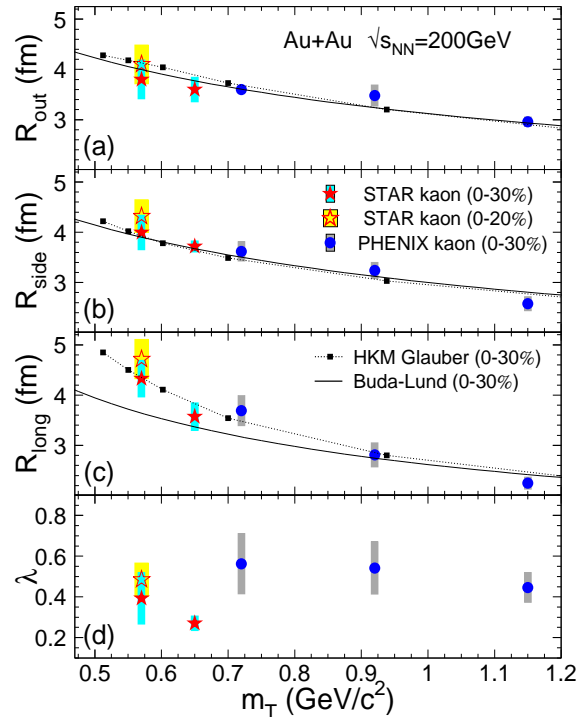

FIG. 4. *(Color online)* Transverse mass dependence of Gaussian radii (a) R_{out}, (b) R_{side} and (c) R_{long} for midrapidity kaon pairs from the 30% most central Au+Au collisions at $\sqrt{s_{NN}}$=200 GeV. STAR data are shown as solid stars; PHENIX data [10] as solid circles (error bars include both statistical and systematic uncertainties). Hydrokinetic model [23] with initial Glauber condition and Buda-Lund model [22] calculations are shown by solid squares and solid curves, respectively. The dotted line between the solid squares is to guide the eye. For comparison purposes, we also plot the result from the 20% most central Au+Au collisions as open stars. Panel (d) shows corresponding experimental values of the Gaussian fit parameter λ.

culations based on the core–halo model [20] employing the STAR ϕ/K^- ratio [21] yields a maximum 15–20% decrease in λ at low transverse momenta. Neither of those two effects has a significant impact on the values of the extracted Gaussian radii.

Figure 4 shows the dependence of the Gaussian radii in LCMS ($R_{out}=R_x/\gamma$, $R_{side}=R_y$ and $R_{long}=R_z$; γ is the kinematic Lorentz boost in the outward direction from the LCMS to the PCMS frame) as a function of transverse mass $m_\mathrm{T} = (m^2 + k_\mathrm{T}^2)^{1/2}$ obtained from the fits to the 3D correlation functions from STAR data (stars). The error bars on the STAR data are dominated by systematic uncertainties from particle identification and momentum resolution. The Gaussian radii for PHENIX kaon data [10] (solid circles) are also shown, with the error bars representing statistical and systematic uncertainties combined. The model calculations from the Buda-Lund model [22] and from the hydrokinetic model (HKM) [23] are shown as solid curves and solid squares, respectively. While the HKM provides a full microscopic transport simulation of hydrodynamic expansion of the system followed by dynamic decoupling, the Buda-Lund model is a pure analytical solution of the perfect fluid hydrodynamics.

TABLE I. Parameters obtained from the 3D Gaussian source function fits for the different datasets. The first errors are statistical, the second errors are systematic.

Year	2004+2007	2004	
Centrality	0%–20%	0%–30%	
k_T [GeV/c]	0.2–0.36	0.2–0.36	0.36–0.48
R_x [fm]	4.8±0.1±0.2	4.3±0.1±0.4	4.5±0.2±0.3
R_y [fm]	4.3±0.1±0.1	4.0±0.1±0.3	3.7±0.1±0.1
R_z [fm]	4.7±0.1±0.2	4.3±0.2±0.4	3.6±0.2±0.3
λ	0.49±0.02±0.05	0.39±0.01±0.09	0.27±0.01±0.04
χ^2/ndf	497/289	316/283	367/283

The latter describes the Gaussian radii of charged pions from Au+Au collisions [24] at the same energy and centrality as our kaon data over the whole $0.30 \leq m_T \leq 1.15$ GeV/c^2 interval [22]. Because the exact m_T–scaling is an inherent feature of perfect fluid hydrodynamics, the Buda-Lund model predicts that the kaon and pion radii fall on the same curve.

From Figure 4 it is seen that the Gaussian radii for the kaon source function display a monotonic decrease with increasing transverse mass m_T from the STAR data at low m_T to the PHENIX data at higher m_T, as do the model calculations of Buda-Lund and HKM. The Gaussian radii in the outward and sideward directions are adequately described by both models over the whole interval. However, there is a marked difference between the HKM and the Buda-Lund predictions in the longitudinal direction, with the deviation becoming prominent for $m_T < 0.7$ GeV/c^2 where the new STAR data reside. Our measurement at $0.2 \leq k_T \leq 0.36$ GeV/c clearly favors the HKM model as more representative of the expansion dynamics of the fireball, despite the fact that the Buda-Lund model describes pion data in all three directions. Hence, exact m_T–scaling of the Gaussian radii in the longitudinal direction between kaons and pions observed at lower energies [25] is not supported by our measurements.

V. CONCLUSIONS

In summary the STAR Collaboration has extracted the 3D source function for midrapidity, low transverse momentum kaon pairs from central Au+Au collisions at $\sqrt{s_{NN}}$=200 GeV via the method of Cartesian surface-spherical harmonic decomposition. The source function is essentially a 3D Gaussian in shape. Comparison with Therminator model calculations indicates that kaons are emitted from a fireball whose transverse dimension and lifetime are consistent with those extracted with two-pion interferometry. However, the 3D source function shapes for kaons and pions are very different. The narrower shape observed for the kaons indicates a much smaller role of long-lived resonance decays and/or of the exponential emission duration width $\Delta\tau$ on kaon emission. The Gaussian radii for the kaon source function display a monotonic decrease with increasing transverse mass m_T over the interval $0.55 \leq m_T \leq 1.15$ GeV/c^2. In the outward and sideward directions, this decrease is adequately described by m_T–scaling. However, in the longitudinal direction, the scaling is broken. The results are in favor of the hydro-kinetic predictions [23] over pure hydrodynamical model calculations.

ACKNOWLEDGEMENTS

[1] I. Arsene *et al.* (BRAHMS Collaboration), Nucl. Phys. A **757**, 1 (2005).

[2] B. B. Back *et al.* (PHOBOS Collaboration), Nucl. Phys. A **757**, 28 (2005).

[3] J. Adams *et al.* (STAR Collaboration), Nucl. Phys. **A 757**, 102 (2005).

[4] K. Adcox *et al.* (PHENIX Collaboration), Nucl. Phys. A **757**, 184 (2005).

[5] Y. Aoki, G. Endrodi, Z. Fodor, S. D. Katz and K. K. Szabo, Nature (London) **443**, 675 (2006).

[6] M. A. Lisa, S. Pratt, R. Soltz and U. Wiedemann, Annu. Rev. Nucl. Part. Sci. **55**, 357 (2005).

[7] P. Danielewicz and S. Pratt, Phys. Lett. **B 618**, 60 (2005).

[8] P. Danielewicz and S. Pratt, Phys. Rev. C **75**, 034907 (2007).

[9] S. Afanasiev *et al.* (PHENIX Collaboration) Phys. Rev. Lett. **100**, 232301 (2008).

[10] S. Afanasiev *et al.* (PHENIX Collaboration) Phys. Rev. Lett. **103**, 142301 (2009).

[11] K. H. Ackermann *et al.* (STAR Collaboration), Nucl. Instrum. Methods Phys. Res., Sect. A **499**, 624 (2003).

[12] R. Lednicky, Phys. Part. Nucl. **40**, 307 (2009).

[13] B. I. Abelev *et al.* (STAR Collaboration), Phys. Rev. C **74**, 054902 (2006).

[14] R. Lednicky and M. I. Podgoretsky, Yad. Fiz. **30**, 837 (1979); [Sov. J. Nucl. Phys. **30**, 432 (1979)].

[15] A. Kisiel, T. Taluc, W. Broniowski and W. Florkowski, Comput. Phys. Commun. **174**, 669 (2006).

[16] A. Kisiel, Braz. J. Phys. **37**, 917 (2007).

[17] B. I. Abelev *et al.* (STAR Collaboration), Phys. Rev. C **79**, 034909 (2009).

[18] A. Kisiel *et al.*, Phys. Rev. C **73** 064902 (2006).

[19] R. Lednicky and T. B. Progulova, Z. Phys. C **55** 295 (1992).

[20] S. E. Vance, T. Csorgo and D. Kharzeev, Phys. Rev. Lett. **81**, 2205 (1998).

[21] J. Adams *et al.* (STAR Collaboration), Phys. Lett. B **612**, 181 (2005).

[22] M. Csanad and T. Csorgo, Acta Phys. Polon. Supp. **1**, 521 (2008).

[23] I. A. Karpenko and Y. M. Sinyukov, Phys. Rev. C **81**, 054903 (2010).

[24] S. S. Adler *et al.* (PHENIX Collaboration), Phys. Rev. Lett. **93**, 152302 (2004).

[25] S. V. Afanasiev *et al.*, Phys. Lett. B **557**, 157 (2003).